Chemical Short-Range Order in Selenide and Telluride Glasses

I. Pethes, R. Chahal, Virginie Nazabal, C. Prestipino, A. Trapananti, S. Michalik, P. Jóvári

THE JOURNAL OF PHYSICAL CHEMISTRY B

Article

pubs.acs.org/JPCB

Chemical Short-Range Order in Selenide and Telluride Glasses

Ildikó Pethes,[*,†] Radwan Chahal,[‡,⊥] Virginie Nazabal,[‡] Carmelo Prestipino,[‡] Angela Trapananti,[§,#] Stefan Michalik,[∥] and Pál Jóvári[†]

[†]Wigner Research Centre for Physics, Hungarian Academy of Sciences, P.O. Box 49, H-1525 Budapest, Hungary

[‡]Institut Sciences Chimiques de Rennes, UMR-CNRS 6226, Campus de Beaulieu, Université de Rennes 1, 35042 Rennes Cedex, France

[§]CNR, Istituto Officina dei Materiali, OGG c/o ESRF, F-38043 Grenoble, France

[∥]Diamond Light Source Ltd., Harwell Science and Innovation Campus, OX11 0DE Didcot, Oxfordshire, U.K.

ABSTRACT: The structure of $Ge_{20}Sb_xSe_{80-x}$ (x = 5, 15, 20) glasses was investigated by neutron diffraction, X-ray diffraction, and extended X-ray fine structure measurements at the Ge, Sb, and Se K-edges. For each composition, large-scale structural models were obtained by fitting simultaneously the experimental data sets in the framework of the reverse Monte Carlo simulation technique. It was found that the structures of these glasses can be described mostly by the chemically ordered network model. Ge−Se and Sb−Se bonds are preferred; Se−Se bonds in the Se-poor composition (x = 20) and M−M (M = Ge, Sb) bonds in strongly Se-rich glass (x = 5) are not needed. The quality of the fits was significantly improved by introducing Ge−Ge bonding in the nearly stoichiometric composition (x = 15), showing a violation of chemical ordering. The structure of $Ge_{20}Sb_xSe_{80-x}$ was compared to that of several glasses from the three analogous systems (Ge−As−Se, Ge−As−Te, Ge−Sb−Te), and it was found that chemical short-range order becomes more pronounced upon substituting As with Sb and Se with Te. Ge−As−Se glasses behave as random covalent networks over a very broad composition range. Chemical short-range order and disorder coexist in both Te-rich and Te-poor Ge−As−Te glasses, whereas amorphous $Ge_{14}Sb_{29}Te_{57}$ and $Ge_{22}Sb_{22}Te_{56}$ are governed by strict chemical preferences.

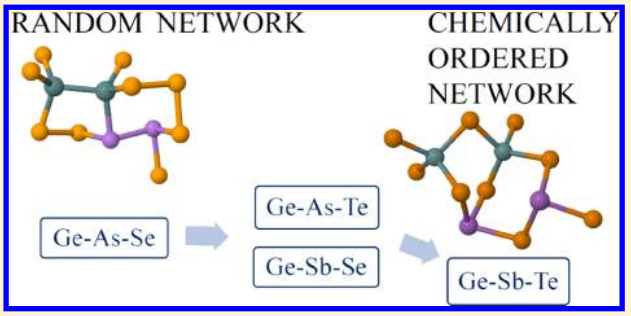

1. INTRODUCTION

Chalcogenide glasses based on chalcogen elements (S, Se, or Te) covalently bonded with other network-forming elements (such as Ge, As, Sb) in binary or multicomponent systems are actively studied because of their prominent optical properties for applications. They have, for example, a wide transparency window from the visible to the mid-infrared range,[1] high linear and nonlinear refractive indices,[2−4] and unique photosensitivities.[5] Chalcogenide glasses are attractive materials in photonics,[4] for instance, for mid-infrared supercontinuum generation[6] or as phase-change materials for rewritable data storage.[7,8] Chalcogenide glass optical fibers and integrated waveguides can be widely applied to ultrafast all-optical switching in telecommunication,[9,10] for the Raman or Brillouin ONL effect,[11,12] or as chemical or biomedical sensors.[13−17]

The 14−15−16 selenides, namely, the Ge−As−Se and Ge−Sb−Se systems, have large glass-forming regions,[18] which leads to the possibility of tuning their physical and optical properties in broad ranges by adjusting their chemical compositions. Among the commercially available infrared optical materials, several Ge−As−Se glasses, such as GASIR ($Ge_{22}As_{20}Se_{58}$) or AMTIR-1 ($Ge_{33}As_{12}Se_{55}$), are used. Because of the toxicity of arsenic, the use of antimony is beneficial, for example, in biomedical applications.[19] Furthermore, the substitution of As with Sb, which has a higher polarizability, may increase the linear and nonlinear indices.[20−24] The presence of Sb reduces the photosensitivity of the material, producing a more stable and stronger network structure.[25,26]

The 14−15−16 telluride glasses have smaller glass-forming regions, but their significances are similarly high: Ge−Sb−Te alloys (e.g., $Ge_{22}Sb_{22}Te_{56}$, $Ge_{38}Sb_{10}Te_{52}$) are broadly used as recording materials for rewritable optical memories (optical DVDs and phase-change random-access memories).[27] Ge−As−Te glasses are more stable against crystallization[28] and have applications as optical fibers[29] or bio-optical sensors.[30]

The structure of chalcogenide glasses can be described as a covalently connected network of the participant elements. According to the Mott rule,[31] the total coordination number of the elements (N_i) is 8-N, where N is the number of s and p electrons in the valence shell of the ith element. For Ge−As(Sb)−Se(Te) glasses, this means that the Ge, As(Sb), and Se(Te) atoms have four, three, and two nearest neighbors, respectively. This rule has been verified for all participating elements in Ge−As−Se,[32−34] Ge−As−Te,[35] and Ge−Sb−Te.[36,37] There is less evidence for the validity of the Mott rule

Received: June 14, 2016
Revised: August 1, 2016
Published: August 1, 2016

DOI: 10.1021/acs.jpcb.6b05996
J. Phys. Chem. B 2016, 120, 9204−9214

Table 1. Mass Densities, Number Densities, Glass-Transition Temperatures, and Fitted Data Sets of the Investigated Ge−Sb−Se Glass Compositions

nominal composition	exact composition	mass density (±0.001, g/cm^3)	number density (atoms Å^{-3})	T_g (±2, °C)	fitted data sets
$Ge_{20}Sb_5Se_{75}$	$Ge_{20.8}Sb_5Se_{74.2}$	4.477	0.03379	192	ND; XRD; Ge-, Se-EXAFS
$Ge_{20}Sb_{15}Se_{65}$	$Ge_{20.2}Sb_{15.1}Se_{64.7}$	4.723	0.03380	272	ND; XRD; Ge-, Sb-, Se-EXAFS
$Ge_{20}Sb_{20}Se_{60}$	$Ge_{20.4}Sb_{20.4}Se_{59.2}$	4.898	0.03414	253	ND; XRD; Ge-, Sb-, Se-EXAFS

in Ge−Sb−Se glasses: ab initio molecular dynamics simulations have shown that they roughly follow this rule.[38]

In the topologically ordered model,[39−41] both homonuclear and heteronuclear bonds are allowed, and the mean coordination number (defined as the sum of the products of the coordination numbers and concentrations of the participant elements) is often used to describe the composition changes leading to coordination and structural modifications affecting the physical properties. In the chemically ordered network model (CONM),[42,43] heteronuclear Ge−Ch and As(Sb)−Ch (Ch = Se, Te) bonds are preferable; the stoichiometric system can be built from only $GeCh_{4/2}$ and $As(Sb)Ch_{3/2}$ units, whereas homonuclear Ch−Ch bonds exist in Ch overstoichiometric (Ch-rich) systems, and bonds between Ge and As(Sb) (Ge−Ge, Ge−As(Sb), Sb−Sb, or As−As) exist in Ch understoichiometric (Ch-poor) systems.

The validity of these models is controversial. There are several experimental studies in which the chemically ordered network is reported (e.g., GeAsSe,[32,44] GeSbSe,[45−48] GeSbTe[36,37]); however, there are also publications on deviations from the above model (e.g., GeAsSe,[33,34] GeSbSe,[23,49] GeAsTe[35,50]).

In this article, we report our results on the short-range order in Ge−Sb−Se systems. Compositions from the Se-rich, nearly stoichiometric, and Se-poor domains are investigated. Structural models are obtained by fitting neutron diffraction (ND), X-ray diffraction (XRD), and extended X-ray absorption fine structure (EXAFS) measurements simultaneously with the reverse Monte Carlo (RMC) simulation technique. Short-range order parameters, bond lengths, and coordination numbers are presented. Results are compared to those for other Ge−X−Ch glasses (X = As, Sb) in the framework of the models mentioned above.

2. EXPERIMENTAL METHODS

2.1. Glass Synthesis and Characterization. $Ge_{20}Sb_xSe_{80-x}$ (x = 5, 15, 20) glasses were synthesized from commercial chemical reagents (Ge, Sb, and Se of 5 N purity) using the conventional melting and quenching technique. Selenium was purified by dynamic and static distillations. All of the elements were weighted and introduced into a silica glass ampoule before sealing it. The elements were melted at 850 °C in a rocking furnace; then, the temperature was decreased to 800 °C, and the samples were kept at this temperature for 10 h. After quenching in water, the glass rods were annealed 20 °C below their glass-transition temperatures over 6 h and finally slowly cooled to room temperature.

A scanning electron microscope with an energy-dispersive X-ray analyzer (JSM 6400; Oxford Link INCA) was used at 20 kV for determination of the chemical composition and homogeneity. The thermal characteristics of the selenide glasses were determined by differential scanning calorimetry (DSC) (Q20 DSC; TA Instruments). DSC measurements were performed with 10 mg powdered samples, which were heated up to 450 °C at heating rate of 10 °C min^{-1} (DSC curves are not shown here). The density of glass was determined using a Mettler Toledo XS64 balance. Disks that were 3 mm in height were placed in the analytical balance, submerged into water, and their densities were determined by averaging three measurements.

The exact compositions of the investigated samples, with their densities and glass-transition temperatures, are shown in Table 1.

2.2. Diffraction Measurements. The ND experiment was carried out on the 7C2 liquid and amorphous diffractometer (LLB Saclay, France). The wavelength of incident radiation was 0.72 Å. Samples were filled into thin-walled (0.1 mm) vanadium sample holders. Raw data were corrected for detector efficiency, background scattering, multiple scattering, and absorption.

The high-energy XRD (HEXRD) experiment was realized at the Joint Engineering, Environmental, and Processing (I12-JEEP) beamline at Diamond Light Source Ltd. (U.K.). Details about the beamline can be found elsewhere.[51] The HEXRD experiment was performed in a monochromatic mode, using a wavelength of 0.14831 Å (energy of 83.595 eV). The beam size was 0.3 × 0.3 mm^2. The precise energy calibration was realized by measuring a fine powder CeO_2 standard (NIST Standard Reference Material 674 b) at different standard-to-detector distances, with knowledge of the relative differences among particular distances following the approach of Hart et al.[52] Then, a standard sample (CeO_2) was measured again to calibrate absolutely the sample-to-detector distance, the orthogonality of the detector with respect to the incoming beam, and the position of the beam center on the detector.

Powder samples were filled into quartz capillaries with a diameter of 1 mm and wall thickness of 0.01 mm. X-ray data were measured in transmission geometry with a large-area 2D detector (Pixium RF4343; Thales). The sample-to-detector distance was 336 mm. The illumination time for obtaining a single diffraction pattern was 20 s. In total, 45 images were collected for each sample. The images were summed up to obtain good statistics at high Q-values. An empty quartz capillary was measured under the same conditions as those for the sample-filled capillaries. 2D patterns were radially integrated into the Q-space to obtain intensity curves $I(Q)$ using the DAWN software.[53] The PDFGetX2 program[54] was applied to extract the total structure factor, $S(Q)$, from the $I(Q)$ curves. First, the empty quartz capillary signal was subtracted from the sample's signal. Sample- and capillary-dependent absorption corrections were applied using cylindrical geometry following the approach of Kendig and Pings.[55] Then, the intensity curve was corrected for Compton scattering and fluorescence. The elastic part of the total scattering signal is extracted and autonormalized into electron units. Finally, structure factor $S(Q)$ is calculated using the Faber−Ziman formalism.[56] The Compton scattering was calculated using the option of the empirical form profile scaled by the Breit−Dirac recoil factor, applying the value of three.[57] Fluorescence was considered to be constant in the whole Q range. Its value (about 1% of the maximal intensity value) was optimized in the way that the

DOI: 10.1021/acs.jpcb.6b05996
J. Phys. Chem. B 2016, 120, 9204−9214

$S(Q)$ curve oscillates around 1 for high Q-values. The normalization constant was calculated by applying the Krogh−Moe−Norman technique,[58,59] using scattering signals covering an interval from $0.6Q_{max}$ to Q_{max}. More details about extraction of the structure factor, $S(Q)$, can be found in the literature.[60] Smaller uncertainties of XRD data corrections may be eliminated by the RMC program,[61] which in its present form allows for rescaling of the structure factor and quadratic background subtraction.

2.3. EXAFS Measurements. EXAFS measurements at the Ge, Se, and Sb K-edges were carried out in the transmission mode at the GILDA-BM08 beamline of the ESRF (Grenoble, France). Monochromatic radiation was obtained with a fixed-exit double crystal monochromator equipped with Si(311) crystals. Two Pd-coated mirrors set at an incidence angle of 3.6 mrad were used for harmonics rejection at Ge and Se K-edges. The intensities of the incident and transmitted beams were recorded using ionization chambers filled with Ar or Kr gas at different pressures to optimize the efficiencies at the different working energies. The samples were finely ground, mixed with cellulose powder, and pressed into pellets. For each composition, the amount of sample was chosen to obtain absorption $\mu t \sim 1.5$ above the selected absorption edge.

The raw absorption spectra were converted to $\chi(k)$ curves using the VIPER program.[62] k^3-weighted $\chi(k)$ signals were first forward Fourier-transformed into r-space using a Kaiser−Bessel window ($\alpha = 1.5$). The k-range of transformation was 1.85−16 Å^{-1} for the Ge and Se edges and 1.85−14 Å^{-1} for the Sb edge. The r-space data were then back-transformed using a rectangular window (over the r-space range 1.1−2.8 Å for Ge and Se edges and 1.4−3.1 Å for Sb-edge data).

Experimental total structure factors ($S(Q)$) and filtered EXAFS curves ($\chi(k)$) are plotted in Figures 1 and 2. Filtered EXAFS data sets are multiplied by k^3 to emphasize high-k oscillations decaying quickly with k.

3. RMC SIMULATIONS

The RMC simulation method[63] is a robust tool for constructing large three-dimensional structural models that are consistent with experimental data, mostly total structure factors obtained from ND and XRD experiments and EXAFS curves. An advantage of the RMC method is that the whole set of experimental curves can be fitted simultaneously. During the simulation, the difference between the experimental and model curves is minimized by random moves of the particles; at the end of the calculation, a particle configuration is obtained that is consistent with all of the experimental data sets within the experimental error. Furthermore, available physical and chemical information such as density, preferred coordination numbers, or bond angles can also be taken into account. From the obtained particle configurations, structural characteristics (partial pair correlation functions, nearest neighbor distributions, coordination numbers, nearest neighbor distances, bond-angle distributions, etc.) can be calculated.

In this study, model configurations were obtained by fitting two or three EXAFS data sets and ND and XRD total structure factors simultaneously by the RMC++ code.[61] The fitted data sets are given in Table 1. The simulation boxes contained 7500 atoms in the test runs and 20 000 atoms in the final runs used for detailed analysis. Initial configurations were obtained by placing the atoms randomly in the simulation box and moving them around until their separations were higher than the minimum interatomic (cutoff) distances. Ge−Se and Sb−Se bonds were always allowed, whereas the necessity of the other bonds was tested by forbidding them in different combinations.

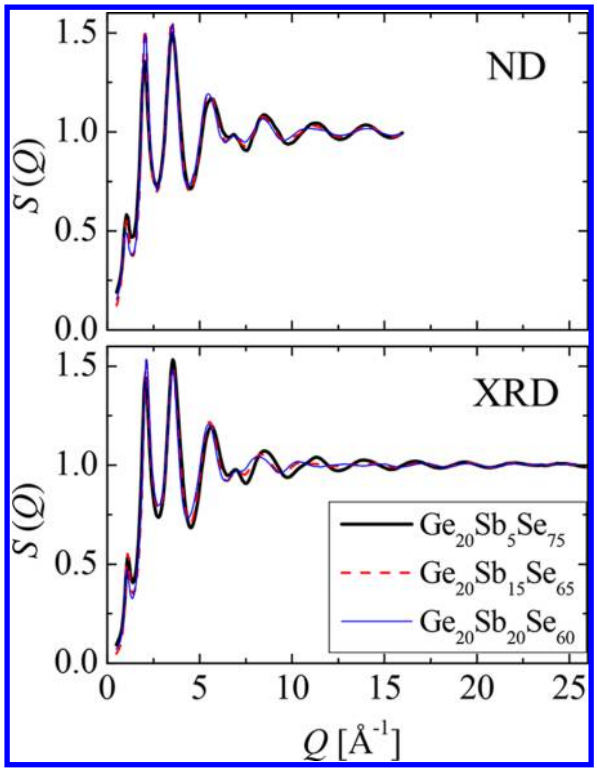

Figure 1. ND and XRD structure factors for the Ge−Sb−Se samples. (Thick solid lines: $Ge_{20}Sb_5Se_{75}$, dashed lines: $Ge_{20}Sb_{15}Se_{65}$, thin solid lines: $Ge_{20}Sb_{20}Se_{60}$ composition.)

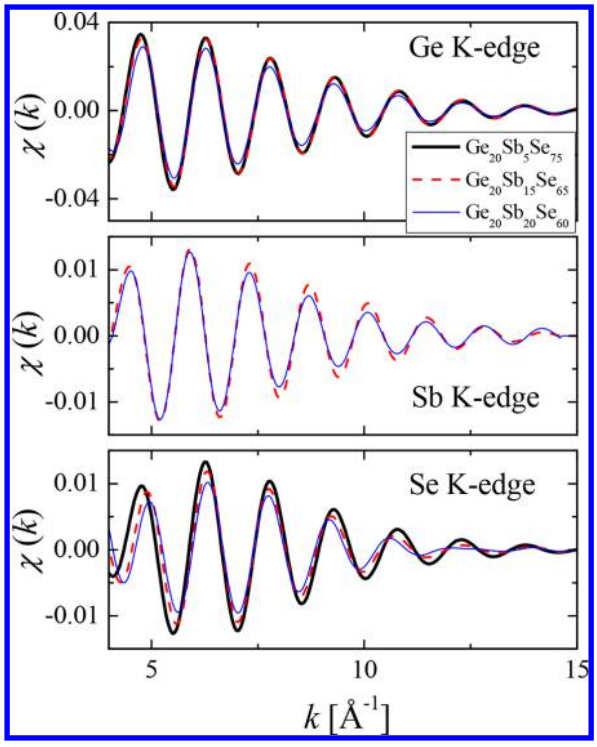

Figure 2. Filtered Ge K-edge, Sb K-edge, and Se K-edge EXAFS spectra for the Ge−Sb−Se samples. (Thick solid lines: $Ge_{20}Sb_5Se_{75}$, dashed lines: $Ge_{20}Sb_{15}Se_{65}$, thin solid lines: $Ge_{20}Sb_{20}Se_{60}$ composition.)

DOI: 10.1021/acs.jpcb.6b05996
J. Phys. Chem. B 2016, 120, 9204−9214

Boxes containing 7500 atoms were also used to optimize the cutoffs. The final values are shown in Table 2. Number densities are listed in Table 1.

Table 2. Minimum Interatomic Distances (Cutoffs) Applied in Simulation Runs (in Å)

pair	Ge−Ge	Ge−Sb	Ge−Se	Sb−Sb	Sb−Se	Se−Se
bond is allowed	2.2	2.5	2.15	2.6	2.4	2.1
bond is forbidden	2.9	2.9		3.15		2.9

EXAFS backscattering coefficients were calculated using the FEFF8.4 program.[64] The S_0^2 values were 0.954, 0.925, and 0.911 for Ge, Sb, and Se, respectively. For details of the RMC-type fitting of EXAFS data, we refer to Winterer.[65] Among the usual EXAFS fitting parameters of a shell (coordination number, peak position, peak width, E_0 correction, see, e.g., the paper of Klementev[66]) the first three are naturally described by the position and shape of the first peak of the corresponding partial pair correlation function. On the other hand, shell-dependent E_0 corrections used to eliminate the shift of the calculated phases and amplitudes are not taken into account by the present RMC code. To minimize this source of error, RMC fits of EXAFS data in most cases start at around 4.5 $Å^{-1}$, where the usual uncertainties of the energy scale have a negligible effect on structural parameters. High E_0 values (~10 eV or higher) may cause persisting, but monotonically decreasing, phase shifts between the experiment and model curve above 5−6 $Å^{-1}$. This type of shift can be eliminated by readjusting manually the *k*-scale of the calculated backscattering curves. (It should be emphasized that the phase shift caused by improper minimum interatomic values is usually not monotonically decreasing and is accompanied by a sizeable amplitude mismatch in most cases.)

The initial sigma parameters used to calculate the RMC cost function[63] were reduced in three steps to 5×10^{-4} for the diffraction data sets and $1-2.5 \times 10^{-5}$ for the EXAFS data sets. The number of accepted moves was typically around $1-2 \times 10^7$.

In the course of the test runs, at first a reference model was obtained for every composition by carrying out a simulation in which all bond types (Ge−Se, Sb−Se, Ge−Ge, Ge−Sb, Sb−Sb, and Se−Se) were allowed, and coordination constraints were used only to avoid unrealistically high or low values of the coordination numbers (usually outside the range $N_{Mott} \pm 2$, where N_{Mott} is the coordination number predicted by the Mott rule) or the presence of atoms without any bonds.

After this reference simulation, several dedicated runs were carried out, in which Ge−Se and Sb−Se bonds were always allowed, whereas bonding among Ge−Ge, Ge−Sb, Sb-Sb, and Se−Se atoms was forbidden in various combinations. In addition, coordination constraints were also applied in some of these runs (see below). The obtained models were evaluated by their cumulative relative *R*-factors. The relative *R*-factor of a model with respect to that of the reference model is defined by the following equation

$$R_r = \frac{\sqrt{\sum (S_{mod} - S_{exp})^2}}{\sqrt{\sum (S_{mod}^{ref} - S_{exp})^2}} \quad (1)$$

where S_{mod} and S_{exp} are the model and experimental curves (structure factors or EXAFS curves), S_{mod}^{ref} is the structure factor (or EXAFS curve) of the reference model, and the summation runs over the experimental data points. Cumulative relative *R*-factors (R_c) are obtained by averaging the relative *R*-factors of a model.

Coordination constraints were applied to evaluate the validity of the Mott rule in this system. In these simulation runs all Ge, Sb, and Se atoms were forced to have four, three, and two neighbors, respectively (in general, without constraining the *type* of neighbors), and about 90−95% of the atoms were required to satisfy these requirements. In a ternary glass, there can be six nonvanishing N_{ij} average coordination numbers. Using a "Mott-type" constraint (e.g., $N_{Ge} = 4$), the sum of the relevant N_{ij} values is constrained (e.g., $N_{GeSe} + N_{GeGe} + N_{GeSb} = 4$). Forbidden bond types should also be considered as constraints ($N_{ij} = 0$). In the models in which the number of forbidden bond types plus Mott-type constraints is less than six, some (one or more) N_{ij} average coordination numbers can vary. The uncertainty of N_{ij} average coordination numbers was estimated by test calculations in which N_{ij} was treated as a fitting parameter and its value was forced to change systematically (e.g., in ±10% steps). By monitoring the *R*-factors, the range in which N_{ij} is compatible with the experimental data can be determined.

In the final models, Mott-type constraints were applied for all of the components. Ge−Se and Sb−Se bonds were allowed in all compositions, Se−Se bonds had to be allowed in $Ge_{20}Sb_5Se_{75}$ and $Ge_{20}Sb_{15}Se_{65}$, Ge−Ge bonds were present in $Ge_{20}Sb_{15}Se_{65}$ and $Ge_{20}Sb_{20}Se_{60}$, whereas Ge−Sb bonding was found to be significant in $Ge_{20}Sb_{20}Se_{60}$. The choice of bond type will be justified in the following section.

Fits of the five data sets of the $Ge_{20}Sb_{15}Se_{65}$ glass sample for the finally applied model (see below) are shown in Figures 3 and 4. The quality of the fits is similar in the case of the other two, $Ge_{20}Sb_5Se_{75}$ (Se-rich) and $Ge_{20}Sb_{20}Se_{60}$ (Se-poor), glass samples.

4. RESULTS AND DISCUSSION

4.1. Investigation of Ge−Sb−Se Glasses. *4.1.1. Validation of the Mott Rule.* In the first step, the reference model of the three compositions was analyzed. In this model, all types of bonds were allowed and only basic coordination constraints were used to avoid unreasonably high or low coordination numbers. The N_i total (average) coordination numbers of the constituents are shown in Table 3. In the case of germanium and selenium atoms, these values are equal (within 15%) to the values predicted by the Mott rule. In case of the $Ge_{20}Sb_5Se_{75}$ glass sample, the low antimony content and the lack of Sb K-edge EXAFS data allow a less accurate determination of the local environment of Sb. However, in glass compositions containing more antimony, the average coordination of Sb is also close to 3. These observations suggest that the Mott rule is valid for all of the participant elements in these glasses.

The use of the coordination constraints of Ge, Sb, and Se atoms having four, three, and two nearest neighbors, respectively, did not worsen the quality of the fits considerably; thus, these coordination constraints have been used in each model hereafter.

4.1.2. Chemical Order in Ge−Sb−Se Glasses. As has already been mentioned, chemical ordering was investigated by creating models in which bond types were allowed in different combinations. The quality of the fits obtained by the simulation runs was monitored. The partial pair correlation functions of the three glass compositions for the final models are shown in

DOI: 10.1021/acs.jpcb.6b05996
J. Phys. Chem. B 2016, 120, 9204−9214

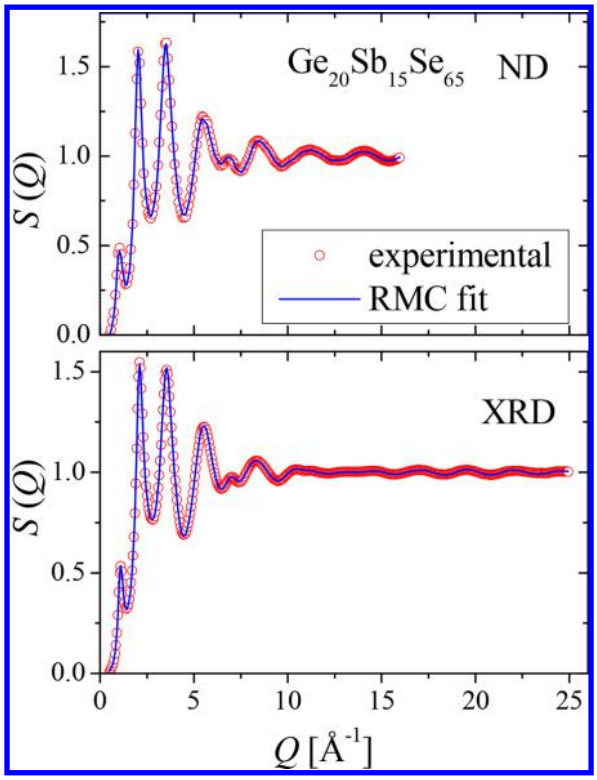

Figure 3. ND and XRD structure factors (symbols) and fits (lines) for the final model (see text) of the $Ge_{20}Sb_{15}Se_{65}$ sample.

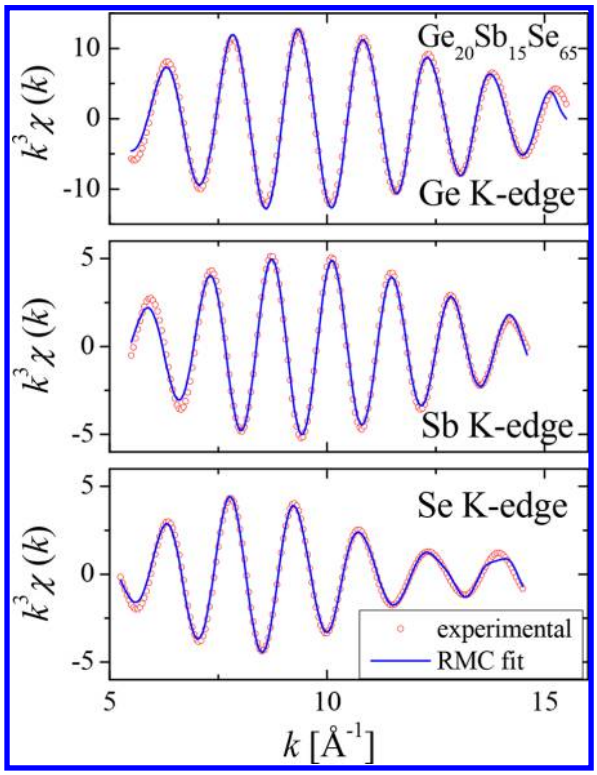

Figure 4. k^3-weighted, filtered EXAFS spectra (symbols) and fits (lines) for the final model (see text) of the $Ge_{20}Sb_{15}Se_{65}$ sample.

Figure 5. Coordination numbers and nearest neighbor distances are presented in Tables 4 and 5.

The experimental data sets of the selenium-rich $Ge_{20}Sb_5Se_{75}$ sample can be fitted well when all of the bonds between

Table 3. Average Coordination Numbers Obtained for the Reference Model[a]

	glass composition		
	$Ge_{20}Sb_5Se_{75}$	$Ge_{20}Sb_{15}Se_{65}$	$Ge_{20}Sb_{20}Se_{60}$
N_{Ge}	3.57	3.68	3.61
N_{Sb}	2.09	2.6	2.84
N_{Se}	2.3	2.18	2.02

[a]That is, the test model in which all of the bonds are allowed and the coordination numbers are not constrained to follow Mott's rule.

nonchalcogen elements are forbidden and only Ge−Se, Sb−Se, and Se−Se bonds are allowed. The mean Ge−Se and Se−Se bond distances (2.37 and 2.34 Å, respectively) are around the values found in binary and ternary glasses using ND with isotopic substitution,[67] EXAFS,[32,44] or the combination of high-energy XRD and EXAFS[33,34,68] (Ge−Se: 2.35−2.37 Å, Se−Se: 2.32−2.40 Å). The Sb−Se bond length (2.57 Å) is somewhat lower than that observed earlier by EXAFS[25] (2.62 Å) and pulsed ND[69] (2.64 Å). The quality of the fits is not improved by allowing the nonchalcogen−nonchalcogen bonds. This shows that the structure of this glass consists of $GeSe_{4/2}$ tetrahedral and $SbSe_{3/2}$ pyramidal units connected by Se atoms or Se−Se-chains, as can be expected from the CONM.

The same bonds (Ge−Se, Sb−Se, and Se−Se) were expected in the nearly stoichiometric (slightly Se-rich) $Ge_{20}Sb_{15}Se_{65}$ composition. Simulation runs with different models showed that Sb−Sb and Ge−Sb bonds can be avoided, but the elimination of Ge−Ge bonds causes a significant increase in the *R*-factors of the experimental data sets (cumulative relative *R*-factor R_c = 1.32). The obtained Ge−Ge mean bond distance (2.43 Å) agrees with the value found for $GeSe_2$ glass.[67] The Ge−Se and Se−Se bond lengths are the same as those in the $Ge_{20}Sb_5Se_{75}$ sample, whereas the Sb−Se bond distance (2.60 Å) is somewhat closer to the value from the literature.[25,69] The structure of this glass consists mainly of $GeSe_{4/2}$ and $SbSe_{3/2}$ units, as that in the Se-rich sample, but the presence of $Se_{3/2}Ge−GeSe_{3/2}$ blocks is not negligible. The average number of Se−Se bonds (N_{SeSe} = 0.4) is also higher than the value given by the CONM (0.05).

A similar behavior was detected by Raman scattering measurements (Figure 7 in Wei et al.[46]) in the $Ge_xSb_{15}Se_{85-x}$ samples, where the authors discovered that the percentage of homonuclear bonds has a minimum at the stoichiometric composition (x = 20.83), but its value is not zero: there are homonuclear bonds in the stoichiometric samples as well. The existence of homonuclear bonds in stoichiometric compositions was also reported by Olivier and co-workers.[23]

The presence of nonchalcogen−nonchalcogen bonds is expected in Se-poor $Ge_{20}Sb_{20}Se_{60}$ glass. Nevertheless, simulation runs showed that Sb−Sb bonds can be eliminated in this composition, whereas Ge−Ge bonds and Ge−Sb bonds are necessary to get reasonably good fits. The Ge−Sb bond length (r_{GeSb} = 2.64 Å) is close to the value reported in Ge−Sb−S glasses[70] (2.65 Å). The uncertainty of the Ge−Ge coordination number is relatively high (−0.6 + 0.1), but complete elimination of this bond type increases the *R*-factor significantly (with an average of 10%). Although the probability of Se−Se bond formation is certainly reduced, Se−Se bonds have also been explored but the value of the corresponding coordination number is close to the sensitivity of our approach.

To conclude, the structure of glassy $Ge_{20}Sb_{20}Se_{60}$ glass is in line with that from the CONM: besides $GeSe_{4/2}$ and $SbSe_{3/2}$

DOI: 10.1021/acs.jpcb.6b05996
J. Phys. Chem. B 2016, 120, 9204−9214

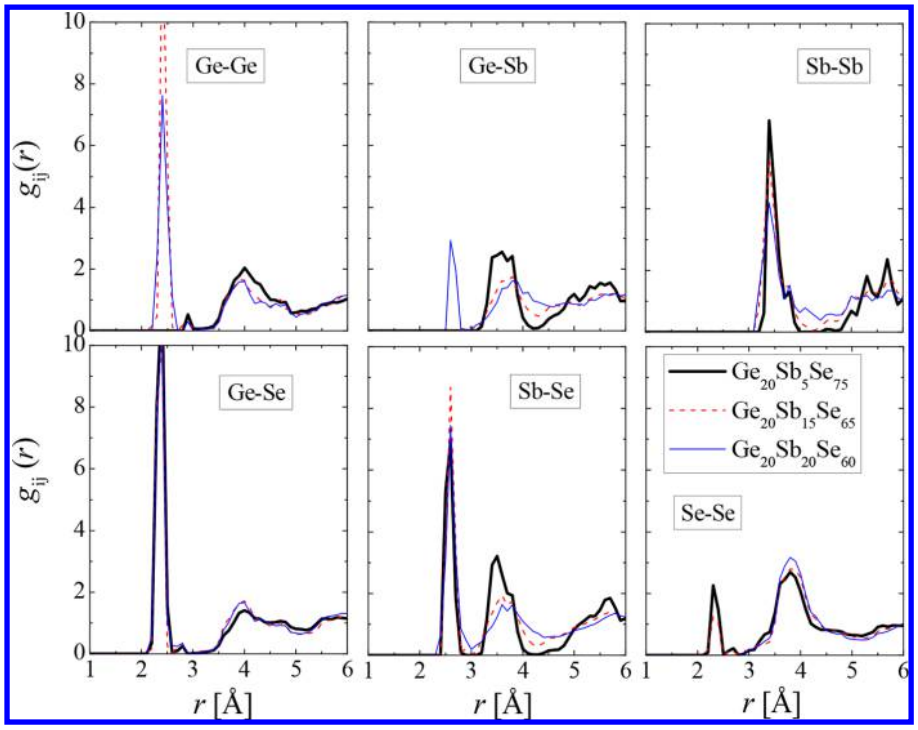

Figure 5. Partial pair correlation functions for the final models (see text) of the Ge−Sb−Se samples. (Thick solid lines: $Ge_{20}Sb_5Se_{75}$, dashed lines: $Ge_{20}Sb_{15}Se_{65}$, thin solid lines: $Ge_{20}Sb_{20}Se_{60}$ composition.)

Table 4. Coordination Numbers of the Different Ge−Sb−Se Compositions[a]

	glass composition		
pair	$Ge_{20}Sb_5Se_{75}$	$Ge_{20}Sb_{15}Se_{65}$	$Ge_{20}Sb_{20}Se_{60}$
Ge−Ge	0	0.98 (±0.4)	0.79 (−0.6 + 0.1)
Ge−Sb	0	0	0.27 (−0.15 + 0.2)
Ge−Se	3.92	2.97 (±0.4)	2.96 (−0.1 + 0.3)
Sb−Ge	0	0	0.27 (−0.15 + 0.2)
Sb−Sb	0	0	0
Sb−Se	2.96	2.96	2.72 (−0.2 + 0.15)
Se−Ge	1.1	0.93 (±0.1)	1.02 (−0.05 + 0.15)
Se−Sb	0.2	0.69	0.94 (±0.1)
Se−Se	0.74	0.4 (±0.1)	0

[a]For "free" values (not fixed by coordination constraints; see Section 3), uncertainties are given in parentheses.

Table 5. Nearest Neighbor Distances (in Å) in the Studied Ge−Sb−Se Glasses

	glass composition		
pair	$Ge_{20}Sb_5Se_{75}$	$Ge_{20}Sb_{15}Se_{65}$	$Ge_{20}Sb_{20}Se_{60}$
Ge−Ge		2.43	2.42
Ge−Sb			2.64
Ge−Se	2.37	2.36	2.36
Sb−Sb			
Sb−Se	2.57	2.60	2.60
Se−Se	2.34	2.34	

units, $Se_{3/2}Ge-Ge(Sb)Se_{3/2}$ blocks are present to compensate for the shortage of selenium.

As the antimony content increases and selenium content decreases, selenium atoms are not able to satisfy the bond requirements of Ge and Sb, and M−M (M = Ge, Sb) bonds appear. Among them, at first Ge−Ge bonds are present, and Sb−Sb bonds can totally be eliminated up to an antimony content of 20 at %.

This highly ordered structure can be observed in the $g_{SbSb}(r)$ partial pair correlation function as well (see Figure 5). Notwithstanding that the first shell around Sb atoms does not contain Sb pairs, the g_{SbSb} function has a well-determined peak around 3.43 Å, which is much higher than the Sb−Sb pair distance (which is expected to be around 2.9 Å).[71] This peak disappears if the XRD dataset is excluded. As the weight of the Sb−Sb pair is much higher in the XRD dataset than that in the other measurements, it seems to be reasonable that this peak is not an artifact of the simulation. Analysis of the final configurations showed that this Sb−Sb distance originates from corner sharing $SbSe_{3/2}$ units.

4.2. Comparison of Ge−As(Sb)−Ch Glasses. In this section, our results for the investigated Ge−Sb−Se glasses are compared to those for three analogous group 14−15−16 systems: Ge−As−Se glasses from ref 34, amorphous Ge−Sb−Te alloys from ref 37, and Ge−As−Te glasses from ref 35. The experimental and simulation methods of the four investigations are nearly identical: diffraction (XRD and, in the case of many compositions, ND) and EXAFS data sets are fitted simultaneously using the RMC simulation technique. The studied compositions are shown in Table 6 and Figure 6.

Coordination numbers of the compared glasses of the four different systems are listed in Table 6. The Mott rule is found to be valid in all chalcogen-rich compositions. However, in the chalcogen-poor region, there may be some violations of the rule. In Ge−As−Se, Ge−Sb−Se, and Ge−Sb−Te systems, it was found that the atoms satisfy the 8-*N* rule. In Ge−As−Te systems, the Te atoms have slightly more than two nearest neighbors in Te-poor compositions,[35] and drastically higher coordination numbers were reported in an earlier publication.[50]

Three of the four systems show characteristics of the CONM. In the tellurium-poor Ge−Sb−Te alloys

DOI: 10.1021/acs.jpcb.6b05996
J. Phys. Chem. B 2016, 120, 9204−9214

Table 6. Coordination Numbers of the Compared Compositions[a]

system	composition	coordination numbers of N_{ij} pairs						total coordination numbers			Ch-poor/-rich
		Ge−Ge	Ge−X	Ge−Ch	X−X	X−Ch	Ch−Ch	Ge	X	Ch	
Ge−Sb−Se	$Ge_{20}Sb_5Se_{75}$	0(1.29)	0(0.23)	3.92(2.40)	0(0.18)	2.96(1.81)	0.74(1.25)	3.92	2.96	2.04	0.27
	$Ge_{20}Sb_{15}Se_{65}$	0.98(1.24)	0(0.69)	2.97(2.02)	0(0.52)	2.96(1.52)	0.40(1.03)	3.95	2.96	2.02	0.03
	$Ge_{20}Sb_{20}Se_{60}$	0.79(1.27)	0.27(0.95)	2.96(1.80)	0(0.7)	2.72(1.34)	0(0.88)	4.02	2.99	1.96	−0.14
Ge−As−Se	$Ge_{10}As_{10}Se_{80}$	1.07(0.69)	0.62(0.53)	2.35(2.81)	0.32(0.41)	2.16(2.16)	1.49(1.43)	4.04	3.1	2.05	0.45
	$Ge_{17.5}As_{10}Se_{72.5}$	1.34(1.13)	0.59(0.49)	2.11(2.41)	0.41(0.38)	1.65(1.85)	1.34(1.24)	4.04	3.09	2.08	0.24
	$Ge_{22.5}As_{10}Se_{67.5}$	1.68(1.43)	0.52(0.48)	1.82(2.12)	0.36(0.36)	1.49(1.60)	1.16(1.05)	4.02	3.03	1.99	0.07
	$Ge_{22}As_{20}Se_{58}$	1.46(1.33)	0.88(0.91)	1.69(1.79)	0.66(0.68)	1.41(1.34)	0.93(0.91)	4.03	3.03	2.05	−0.15
	$Ge_{27.5}As_{10}Se_{62.5}$	1.84(1.67)	0.47(0.46)	1.72(1.90)	0.30(0.34)	1.42(1.42)	1.02(0.95)	4.03	3.02	2.01	−0.08
	$Ge_{30}As_{10}Se_{60}$	2.04(1.80)	0.45(0.45)	1.53(1.77)	0.39(0.33)	1.25(1.32)	1.00(0.87)	4.02	2.99	1.98	−0.16
	$Ge_{33}As_{12}Se_{55}$	1.96(1.91)	0.52(0.52)	1.55(1.60)	0.36(0.39)	1.23(1.20)	0.83(0.81)	4.03	3.02	2.03	−0.28
	$Ge_{35}As_{10}Se_{55}$	2.18(2.02)	0.43(0.43)	1.41(1.56)	0.28(0.33)	1.23(1.18)	0.86(0.77)	4.02	3.02	1.98	−0.31
	$Ge_{33}As_{20}Se_{47}$	1.93(1.89)	0.86(0.85)	1.24(1.30)	0.57(0.62)	0.99(0.96)	0.66(0.63)	4.03	2.98	1.95	−0.52
Ge−Sb−Te	$Ge_{14}Sb_{29}Te_{57}$	0.49(0.87)	0.66(1.29)	2.76(1.75)	0(0.96)	2.58(1.31)	0(0.89)	3.91	2.91	1.98	−0.13
	$Ge_{22}Sb_{22}Te_{56}$	0.79(1.23)	0.60(1.01)	2.45(1.60)	0(0.82)	2.53(1.30)	0(0.83)	3.84	3.13	1.99	−0.22
Ge−As−Te	$Ge_{10}As_{10}Te_{80}$	0(0.69)	0(0.52)	4.0(2.78)	0.15(0.39)	2.87(2.10)	1.15(1.40)	4.0	3.02	2.01	0.45
	$Ge_{10}As_{15}Te_{75}$	0(0.67)	0(0.76)	4.03(2.60)	0.43(0.57)	2.60(1.95)	1.01(1.33)	4.03	3.03	2.07	0.34
	$Ge_5As_{55}Te_{40}$	0(0.30)	1.56(2.47)	2.44(1.23)	1.82(1.85)	1.04(0.92)	0.31(0.63)	4.0	3.0	2.06	−0.50
	$Ge_{15}As_{45}Te_{40}$	0(0.84)	1.56(1.95)	2.46(1.23)	1.72(1.50)	0.85(0.95)	0.33(0.67)	4.02	3.09	2.2	−0.51
	$Ge_{20}As_{40}Te_{40}$	0(1.12)	1.89(1.70)	2.11(1.18)	1.37(1.29)	0.72(0.89)	0.33(0.62)	4.0	3.04	2.1	−0.56

[a]The values of the corresponding random (disordered) network are also shown in parentheses. X represents As and Sb atoms, and Ch represents Se and Te atoms. The last column is the chalcogen deficiency/excess (defined in the text). Ge−Sb−Se from this study, Ge−As−Se data from ref 34, Ge−Sb−Te data from ref 37, and Ge−As−Te data from ref 35.

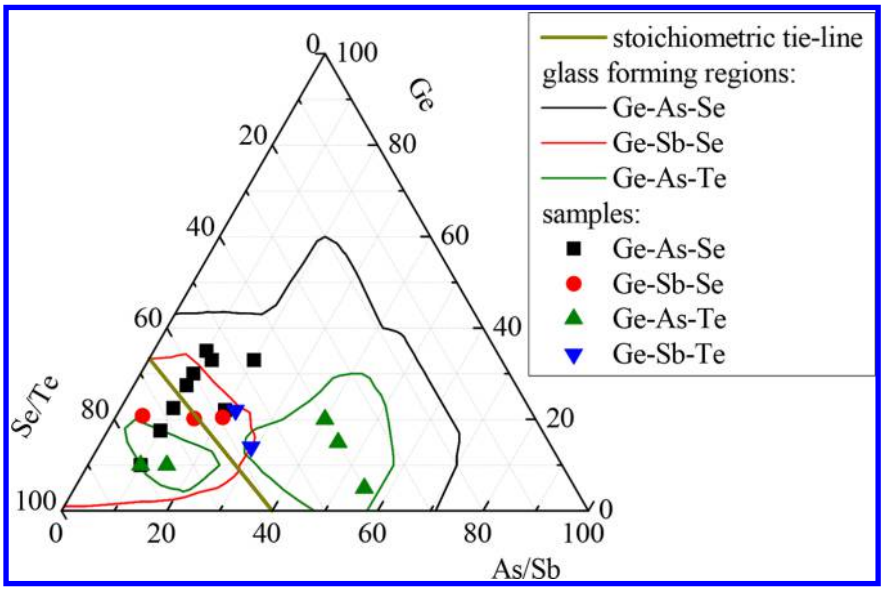

Figure 6. Ternary diagram of the compared 14−15−16 glasses. (Squares: Ge−As−Se, circles: Ge−Sb−Se, upward triangle: Ge−As−Te, downward triangle: Ge−Sb−Te.) The glass-forming regions are shown only schematically. The stoichiometric tie-line is also indicated.

($Ge_{14}Sb_{29}Te_{57}$ and $Ge_{22}Sb_{22}Te_{56}$), there are only Ge−Ge, Ge−Sb, Ge−Ch, and Sb−Ch bonds, similar to those in the Se-poor $Ge_{20}Sb_{20}Se_{60}$ compound.

In Ge−As−Te glasses, there is some chemical ordering as well: in tellurium-rich samples ($Ge_{10}As_{10}Te_{80}$ and $Ge_{10}As_{15}Te_{75}$) the Ge−Ge and Ge−As bonds are missing; the germanium atoms have only tellurium neighbors. However, in these glasses, As−As bonds are present. The disorder is conspicuous in tellurium-poor compositions ($Ge_xAs_{60-x}Te_{40}$, x = 5, 15, 20) too: there are Te−Te bonds even in strongly Te-poor samples. Still, these (Te-poor) glasses keep some remnants of chemical order: Ge−Ge bonds are completely absent.

The family of Ge−As−Se glasses (see Figure 6 and Table 6 for compositions) shows a completely disordered structure. There are Ge−Ge, Ge−As, and As−As bonds in highly selenium-rich compositions and Se−Se bonds in selenium-poor samples.

To compare the chemical ordering of the different glasses in a more quantitative way, the coordination numbers are examined with respect to the coordination numbers of a random network (chemically disordered) configuration. In the

DOI: 10.1021/acs.jpcb.6b05996
J. Phys. Chem. B 2016, 120, 9204−9214

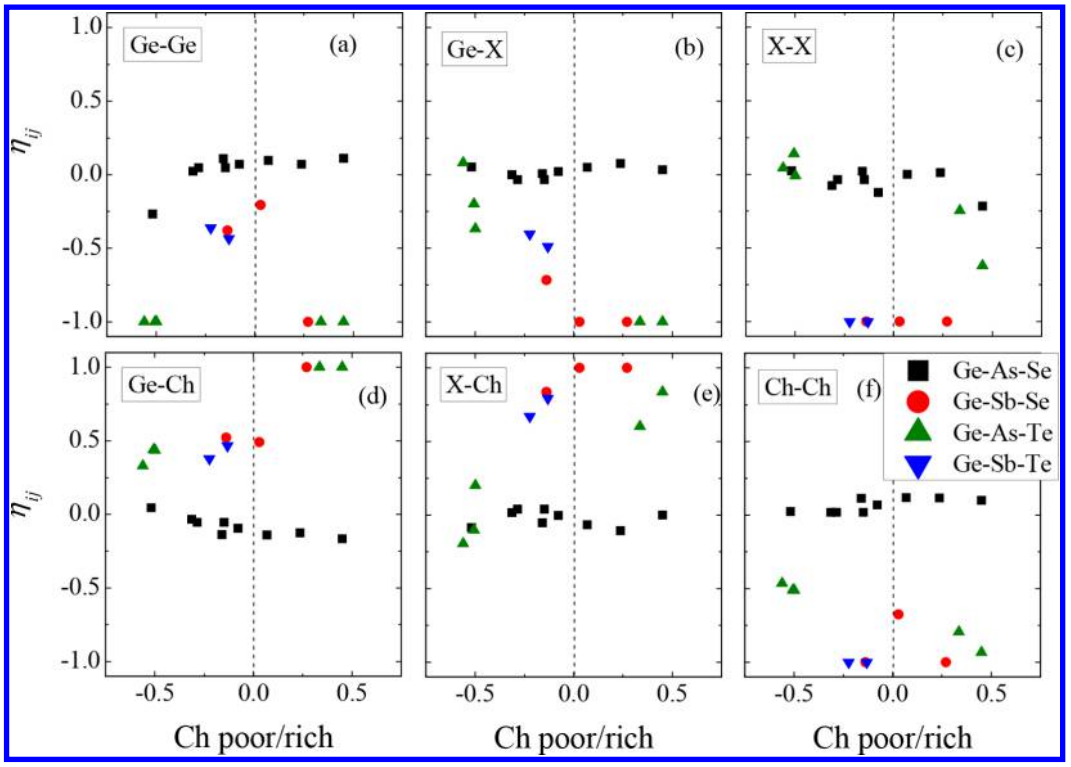

Figure 7. η_{ij} values of the compared glasses. (Squares: Ge−As−Se, circles: Ge−Sb−Se, upward triangle: Ge−As−Te, downward triangle: Ge−Sb−Te.) The compositions are arranged by their chalcogen excess/deficiency (see text). X represents As and Sb atoms, and Ch represents Se and Te atoms. Subfigure (a) shows η_{GeGe}, (b) η_{GeX}, (c) η_{XX}, (d) η_{GeCh}, (e) η_{XCh}, and (f) η_{ChCh}.

case of a random network, the N_{ij}^{r} coordination numbers can be obtained as

$$N_{ij}^{r} = \frac{N_i c_j N_j}{\sum_k c_k N_k} \tag{2}$$

where N_i and c_i are the total coordination number and concentration of the ith component, respectively. N_{ij}^{r} values are also shown in Table 6 (in parentheses).

Deviations from complete chemical disorder can be characterized by a short-range order coefficient

$$\eta_{ij} = \frac{N_{ij} - N_{ij}^{r}}{\eta_{ij}^{0}} \tag{3}$$

where

$$\eta_{ij}^{0} = \begin{cases} N_{ij}^{max} - N_{ij}^{r} & \text{if } N_{ij} \geq N_{ij}^{r} \\ N_{ij}^{r} - N_{ij}^{min} & \text{if } N_{ij} \leq N_{ij}^{r} \end{cases} \tag{4}$$

N_{ij}^{min} and N_{ij}^{max} are the possible minimum and maximum values of the N_{ij} coordination numbers, respectively: N_{ij}^{min} corresponds to the value of the N_{ij} coordination number in a theoretical configuration in which the i−j bonds are the least preferred (that is, i−j pairs are present only in the minimum necessary amount required to satisfy the bond requirements of the i- and j-type elements). This definition takes into account that in off-stoichiometric compositions the presence of "wrong bonds" is not necessarily a sign of chemical disorder. Similarly, N_{ij}^{max} is the value that can be reached if the i−j bond is the most preferred bond (only i−j bonds are formed until the valences of i- or j-type atoms are fully satisfied). These values depend on the total coordination numbers and concentrations as follows

$$N_{ij}^{max} = \begin{cases} N_i & \text{if } c_i N_i \leq c_j N_j \\ \dfrac{c_j N_j}{c_i} & \text{if } c_i N_i \geq c_j N_j \end{cases} \tag{5}$$

$$N_{ij}^{min} = \begin{cases} N_i - \sum_{k \neq j} N_{ik}^{max} & \text{if } N_i > \sum_{k \neq j} N_{ik}^{max} \\ 0 & \text{if } N_i \leq \sum_{k \neq j} N_{ik}^{max} \end{cases} \tag{6}$$

On the basis of the above detailed definition, η_{ij} (order coefficient) is representative of the degree of chemical order of the glass network. It can vary between −1 and 1; η_{ij} is 0 for complete chemical disorder ($N_{ij} = N_{ij}^{r}$). $\eta_{ij} > 0$ means that the i−j bond is preferred, and for the nonpreferred bonds, $\eta_{ij} < 0$.

This order coefficient is similar to the short-range order parameter of Cargill and Spaepen[72] or the Warren−Cowley order parameter.[57,73,74]

The η_{ij} values of the compared glasses are presented in Figure 7. The different compositions are arranged by their chalcogen deficiency/excess (Ch-poor/-rich = $(c_{Ch}N_{Ch} - c_{Ge}N_{Ge} - c_X N_X)/N_{Ch}$, which is positive in chalcogen-rich systems and negative in chalcogen-poor compositions).

In a chemically ordered network, η_{GeCh} and η_{XCh} are expected to be 1 in chalcogen-rich compositions. This is the situation in the Ge−Sb−Se system; however, in Ge−As−Te glass, only η_{GeTe} is equal to 1, whereas η_{AsTe} is 0.84 and 0.60 in $Ge_{10}As_{10}Te_{80}$ and $Ge_{10}As_{15}Te_{75}$, respectively. The presence of As−As bonds necessarily reduces the number of As−Te bonds (see Figure 7c−e). For the Ge−Sb−Te system, the two studied compositions are chalcogen-poor.

DOI: 10.1021/acs.jpcb.6b05996
J. Phys. Chem. B 2016, 120, 9204−9214

In the chalcogen-poor region, η_{GeCh} and η_{XCh} cannot be equal to 1 simultaneously. The fact that the values of η_{SbCh} (∼0.7−0.8) are higher than those of η_{GeCh} (∼0.4−0.5) in $Ge_{20}Sb_{20}Se_{60}$ as well as in $Ge_{14}Sb_{29}Te_{57}$ and $Ge_{22}Sb_{22}Te_{56}$ (together with the $\eta_{SbSb} = -1$ values) suggests that the structures of these glasses are more ordered around antimony than that around germanium. In Te-poor Ge−As−Te glasses, a similar comparison of η_{AsTe} and η_{GeTe} shows that the system tends toward chemical disorder in the case of arsenic, whereas the structure is more ordered around germanium, with $\eta_{GeTe} \sim 0.35-0.45$ and $\eta_{GeGe} \sim -1$. In the Ge−As−Se system, η_{GeSe} and η_{AsSe} are close to 0, indicating the lack of chemical ordering.

The η_{ChCh} values (see Figure 7f) of the Ge−Sb−Te glasses and of two of the glasses from the Ge−Sb−Se compositions are equal to −1, which clearly shows that chalcogen−chalcogen bonds are not preferred in these glasses, as expected from the CONM. The nearly stoichiometric $Ge_{20}Sb_{15}Se_{65}$ composition shows a violation of chemical ordering: the Se−Se coordination number is much lower than the random value ($\eta_{SeSe} \ll 0$) but significantly higher than its minimum value ($\eta_{SeSe} \gg -1$). The arsenic glasses are less ordered: their η_{ChCh} values never go down to −1, even if this value is approached in the Ch-rich domain of the Ge−As−Te system.

The chalcogen−chalcogen bonds are obviously the most important in the Ge−As−Se system, where N_{SeSe} is clearly higher than that in the CONM in both the Se-poor and -rich regions.

According to the CONM, Ge−Ge, Ge−X, and X−X bonds are not expected in chalcogen-rich compositions. In the chalcogen-poor samples, chalcogen deficiency requires the presence of Ge−Ge, X−X, or Ge−X bonds; thus, the η_{GeGe}, η_{XX}, and η_{GeX} values cannot be equal to −1 simultaneously.

In the Ge−Sb−Se and Ge−Sb−Te systems, η_{SbSb} values are equal to −1 for all compositions; only Ge−Ge and Ge−Sb bonds are formed to satisfy the valence requirements. Ge−Sb and Ge−Ge bonds seem to be equally preferred in Ge−Sb−Te, whereas Ge−Ge bonding is more preferred in Ge−Sb−Se glasses.

There is no significant preference among the nonchalcogen−nonchalcogen bonds in Ge−As−Se glasses, although the η_{GeGe} values are slightly higher than those of the other two. In the Ge−As−Te system, there is a definite priority: η_{AsAs} is the highest and η_{GeGe} is the lowest among them. Ge−Ge bonds are totally avoided in these glasses.

From this comparison, it can be concluded that the order in the network structure increases with an increase in the atomic number of the participant elements. The structure of Ge−As−Se glasses is a random network. A more ordered structure is obtained if Sb atoms substitute As atoms. The structures of Ge−Sb−Se glasses in the Se-poor and -rich regions can be described by the CONM, but there is a violation of the chemical order in the nearly stoichiometric composition. Similarly, the substitution of selenium with tellurium increases the chemical order. The structure of Ge−As−Te glasses is chemically more ordered than that of Ge−As−Se glasses: the environment of Ge atoms is perfectly ordered in these glasses. Finally, the investigated Te-poor amorphous Ge−Sb−Te alloys are even more ordered than Ge−As−Te glasses because their structures can completely be described by the CONM.

5. CONCLUSIONS

The structures of $Ge_{20}Sb_5Se_{75}$, $Ge_{20}Sb_{15}Se_{65}$, and $Ge_{20}Sb_{20}Se_{60}$ glasses were investigated by ND, XRD, and EXAFS spectroscopy. Experimental data sets were fitted by the RMC simulation technique. It was showed that all components obey the Mott rule. The structures of these glasses can be described mostly by the CONM: Ge−Se and Sb−Se bonds are preferred; Se−Se bonds in Se-poor and M−M (M = Ge, Sb) bonds in Se-rich compositions are not needed. A violation of the chemical order was observed in the nearly stoichiometric composition. Comparison with other glasses from the 14−15−16 group showed that the chemical order strengthens upon replacing As with Sb and Se with Te.

Se-poor Ge−As−Se glasses can be described as random covalent networks with significant Se−Se bonding in strongly Se-poor compositions. Te−Te bonding is significant but less favored in Te-poor Ge−As−Te glasses, and no Ch−Ch bonds were found in Ch-poor Ge−Sb−Se and Ge−Sb−Te compositions.

Ge−Ge, Ge−As, and As−As bonding is significant in Se-rich Ge−As−Se glasses. Whereas As−As bonds are present in Te-rich Ge−As−Te glasses, Ge−Ge and Ge−As bonds are clearly avoided. Finally, no M−M bonds were found in the Se-rich Ge−Sb−Se glass investigated.

AUTHOR INFORMATION

Corresponding Author

*E-mail: pethes.ildiko@wigner.mta.hu. Tel./Fax: +36 1 392 2589.

Present Addresses

[#](A.T.) CNR, Istituto Officina dei Materiali, Unità di Perugia, c/o Dipartimento di Fisica e Geologia, Università di Perugia, Via A. Pascoli, I-06123 Perugia, Italy.

[⊥](R.C.) Department of Physics, NTNU, NO-7491 Trondheim, Norway.

Notes

The authors declare no competing financial interest.

ACKNOWLEDGMENTS

I.P. and P.J. were supported by NKFIH (National Research, Development and Innovation Office) Grant No. SNN 116198. The assistance of Claudia Pantalei during the ND experiment is greatly acknowledged. We acknowledge the European Synchrotron Radiation Facility for provision of synchrotron radiation facilities. V.N. is thankful to ADEME for PhD funds.

REFERENCES

(1) Sanghera, J. S.; Aggarwal, I. D. Active and Passive Chalcogenide Glass Optical Fibers for IR Applications: A Review. *J. Non-Cryst. Solids* **1999**, *256−257*, 6−16.

(2) Tanaka, K. Optical Nonlinearity in Photonic Glasses. *J. Mater. Sci.: Mater. Electron.* **2005**, *16*, 633−643.

(3) Shimakawa, K.; Kolobov, A.; Elliott, S. R. Photoinduced Effects and Metastability in Amorphous Semiconductors and Insulators. *Adv. Phys.* **1995**, *44*, 475−588.

(4) Zakery, A.; Elliott, S. R. Optical Properties and Applications of Chalcogenide Glasses: A Review. *J. Non-Cryst. Solids* **2003**, *330*, 1−12.

(5) Eggleton, B. J.; Luther-Davies, B.; Richardson, K. Chalcogenide Photonics. *Nat. Photonics* **2011**, *5*, 141−148.

(6) Kubat, I.; Petersen, C. R.; Moller, U. V.; Seddon, A.; Benson, T.; Brilland, L.; Mechin, D.; Moselund, P. M.; Bang, O. Thulium Pumped Mid-Infrared 0.9−9 μm Supercontinuum Generation in Concatenated Fluoride and Chalcogenide Glass Fibers. *Opt. Express* **2014**, *22*, 3959−3967.

(7) Wuttig, M.; Yamada, N. Phase-Change Materials for Rewriteable Data Storage. *Nat. Mater.* **2007**, *6*, 824−832.

DOI: 10.1021/acs.jpcb.6b05996
J. Phys. Chem. B 2016, 120, 9204−9214

(8) Milliron, D. J.; Raoux, S.; Shelby, R. M.; Jordan-Sweet, J. Solution-Phase Deposition and Nanopatterning of GeSbSe Phase-Change Materials. *Nat. Mater.* **2007**, *6*, 352−356.
(9) Asobe, M. Nonlinear Optical Properties of Chalcogenide Glass Fibers and Their Application to All-Optical Switching. *Opt. Fiber Technol.* **1997**, *3*, 142−148.
(10) Gai, X.; Han, T.; Prasad, A.; Madden, S.; Choi, D.-Y.; Wang, R. P.; Bulla, D.; Luther-Davies, B. Progress in Optical Waveguides Fabricated from Chalcogenide Glasses. *Opt. Express* **2010**, *18*, 26635−26646.
(11) Jackson, S. D.; Anzueto-Sánchez, G. Chalcogenide Glass Raman Fiber Laser. *Appl. Phys. Lett.* **2006**, *88*, No. 221106.
(12) Abedin, K. S. Observation of Strong Stimulated Brillouin Scattering in Single-Mode As_2Se_3 Chalcogenide Fiber. *Opt. Express* **2005**, *13*, 10266.
(13) Bureau, B.; Zhang, X. H.; Smektala, F.; Adam, J.-L.; Troles, J.; Ma, H.; Boussard-Plèdel, C.; Lucas, J.; Lucas, P.; Le Coq, D.; et al. Recent Advances in Chalcogenide Glasses. *J. Non-Cryst. Solids* **2004**, *345*−*346*, 276−283.
(14) Anne, M.-L.; Keirsse, J.; Nazabal, V.; Hyodo, K.; Inoue, S.; Boussard-Plèdel, C.; Lhermite, H.; Charrier, J.; Yanakata, K.; Loreal, O.; et al. Chalcogenide Glass Optical Waveguides for Infrared Biosensing. *Sensors* **2009**, *9*, 7398−7411.
(15) Starecki, F.; Charpentier, F.; Doualan, J.-L.; Quetel, L.; Michel, K.; Chahal, R.; Troles, J.; Bureau, B.; Braud, A.; Camy, P.; et al. Mid-IR Optical Sensor for CO_2 Detection Based on Fluorescence Absorbance of Dy^{3+}:$Ga_5Ge_{20}Sb_{10}S_{65}$ Fibers. *Sens. Actuators, B: Chemical* **2015**, *207*, 518−525.
(16) Charrier, J.; Brandily, M.-L.; Lhermite, H.; Michel, K.; Bureau, B.; Verger, F.; Nazabal, V. Evanescent Wave Optical Micro-Sensor Based on Chalcogenide Glass. *Sens. Actuators, B: Chemical* **2012**, *173*, 468−476.
(17) Singh, V.; Lin, P. T.; Patel, N.; Lin, H.; Li, L.; Zou, Y.; Deng, F.; Ni, C.; Hu, J.; Giammarco, J.; et al.*et al.* Mid-Infrared Materials and Devices on a Si Platform for Optical Sensing. *Sci. Technol. Adv. Mater.* **2014**, *15*, No. 014603.
(18) Borisova, Z. U. *Glassy Semiconductors*; Plenum Press: New York, 1981.
(19) Butterworth, J. H.; Jayasuriya, D.; Li, Q. Q.; Furniss, D.; Moneim, N. A.; Barney, E.; Sujecki, S.; Benson, T. M.; Sanghera, J. S.; Seddon, A. B. In Towards Mid-Infrared Supercontinuum Generation: Ge-Sb-Se Mid-Infrared Step-Index Small-Core Optical Fiber, *Proceedings of SPIE*, Optical Fibers and Sensors for Medical Diagnostics and Treatment Applications XIV, San Francisco, California, Feb 20, 2014; Gannot, I., Ed.; Society of Photo-Optical Instrumentation Engineers, 2014; Vol. *8938*, p 89380W.
(20) Němec, P.; Olivier, M.; Baudet, E.; Kalendová, A.; Benda, P.; Nazabal, V. Optical Properties of $(GeSe_2)_{100-x}(Sb_2Se_3)_x$ Glasses in near- and Middle-Infrared Spectral Regions. *Mater. Res. Bull.* **2014**, *51*, 176−179.
(21) Lenz, G.; Zimmermann, J.; Katsufuji, T.; Lines, M. E.; Hwang, H. Y.; Spälter, S.; Slusher, R. E.; Cheong, S.-W.; Sanghera, J. S.; Aggarwal, I. D. Large Kerr Effect in Bulk Se-Based Chalcogenide Glasses. *Opt. Lett.* **2000**, *25*, 254.
(22) Harbold, J. M.; Ilday, F. O.; Wise, F. W.; Aitken, B. G. Highly Nonlinear Ge-As-Se and Ge-As-S−Se Glasses for All-Optical Switching. *IEEE Photonics Technol. Lett.* **2002**, *14*, 822−824.
(23) Olivier, M.; Tchahame, J. C.; Němec, P.; Chauvet, M.; Besse, V.; Cassagne, C.; Boudebs, G.; Renversez, G.; Boidin, R.; Baudet, E.; et al. Structure, Nonlinear Properties, and Photosensitivity of $(GeSe_2)_{100-x}(Sb_2Se_3)_x$ Glasses. *Opt. Mater. Express* **2014**, *4*, 525.
(24) Chen, L.; Chen, F.; Dai, S.; Tao, G.; Yan, L.; Shen, X.; Ma, H.; Zhang, X.; Xu, Y. Third-Order Nonlinearity in Ge−Sb−Se Glasses at Mid-Infrared Wavelengths. *Mater. Res. Bull.* **2015**, *70*, 204−208.
(25) Ganjoo, A.; Jain, H.; Khalid, S.; Pantano, C. G. Structural Modification of Ge−Se Amorphous Films with the Addition of Sb. *Philos. Mag. Lett.* **2005**, *85*, 503−512.
(26) Olivier, M.; Němec, P.; Boudebs, G.; Boidin, R.; Focsa, C.; Nazabal, V. Photosensitivity of Pulsed Laser Deposited Ge-Sb-Se Thin Films. *Opt. Mater. Express* **2015**, *5*, 781.
(27) Yamada, N.; Ohno, E.; Nishiuchi, K.; Akahira, N.; Takao, M. Rapid-Phase Transitions of GeTe-Sb_2Te_3 Pseudobinary Amorphous Thin Films for an Optical Disk Memory. *J. Appl. Phys.* **1991**, *69*, 2849−2856.
(28) Yang, Z.; Lucas, P. Tellurium-Based Far-Infrared Transmitting Glasses. *J. Am. Ceram. Soc.* **2009**, *92*, 2920−2923.
(29) Yang, Z.; Luo, T.; Jiang, S.; Geng, J.; Lucas, P. Single-Mode Low-Loss Optical Fibers for Long-Wave Infrared Transmission. *Opt. Lett.* **2010**, *35*, 3360.
(30) Yang, Z.; Fah, M. K.; Reynolds, K. A.; Sexton, J. D.; Riley, M. R.; Anne, M.-L.; Bureau, B.; Lucas, P. Opto-Electrophoretic Detection of Bio-Molecules Using Conducting Chalcogenide Glass Sensors. *Opt. Express* **2010**, *18*, 26754.
(31) Mott, N. F. Electrons in Disordered Structures. *Adv. Phys.* **1967**, *16*, 49−144.
(32) Sen, S.; Aitken, B. G. Atomic Structure and Chemical Order in Ge-As Selenide and Sulfoselenide Glasses: An X-Ray Absorption Fine Structure Spectroscopic Study. *Phys. Rev. B* **2002**, *66*, No. 134204.
(33) Kaban, I.; Jóvári, P.; Wang, R. P.; Luther-Davies, B.; Mattern, N.; Eckert, J. Structural Investigations of $Ge_5As_xSe_{95-x}$ and $Ge_{15}As_xSe_{85-x}$ Glasses Using X-Ray Diffraction and Extended X-Ray Fine Structure Spectroscopy. *J. Phys.: Condens. Matter* **2012**, *24*, No. 385802.
(34) Pethes, I.; Kaban, I.; Wang, R. P.; Luther-Davies, B.; Jóvári, P. Short Range Order in Ge−As−Se Glasses. *J. Alloys Compd.* **2015**, *623*, 454−459.
(35) Jóvári, P.; Lucas, P.; Yang, Z.; Bureau, B.; Kaban, I.; Beuneu, B.; Bednarčik, J. Short-Range Order in Ge-As-Te Glasses. *J. Am. Ceram. Soc.* **2014**, *97*, 1625−1632.
(36) Jóvári, P.; Kaban, I.; Steiner, J.; Beuneu, B.; Schöps, A.; Webb, A. "Wrong Bonds" in Sputtered Amorphous $Ge_2Sb_2Te_5$. *J. Phys.: Condens. Matter* **2007**, *19*, No. 335212.
(37) Jóvári, P.; Kaban, I.; Steiner, J.; Beuneu, B.; Schöps, A.; Webb, M. Local Order in Amorphous $Ge_2Sb_2Te_5$ and $GeSb_2Te_4$. *Phys. Rev. B* **2008**, *77*, No. 035202.
(38) Opletal, G.; Drumm, D. W.; Petersen, T. C.; Wang, R. P.; Russo, S. P. Ab Initio Comparison of Bonding Environments and Threshold Behavior in $Ge_xAs_{10}Se_{90-x}$ and $Ge_xSb_{10}Se_{90-x}$ Glass Models. *J. Phys. Chem. A* **2015**, *119*, 6421−6427.
(39) Phillips, J. C. Topology of Covalent Non-Crystalline Solids I: Short-Range Order in Chalcogenide Alloys. *J. Non-Cryst. Solids* **1979**, *34*, 153−181.
(40) Thorpe, M. F. Continuous Deformations in Random Networks. *J. Non-Cryst. Solids* **1983**, *57*, 355−370.
(41) Tanaka, K. Structural Phase Transitions in Chalcogenide Glasses. *Phys. Rev. B* **1989**, *39*, 1270−1279.
(42) Lucovsky, G.; Galeener, F. L.; Keezer, R. C.; Geils, R. H.; Six, H. A. Structural Interpretation of the Infrared and Raman Spectra of Glasses in the Alloy System $Ge_{1-x}S_x$. *Phys. Rev. B* **1974**, *10*, 5134−5146.
(43) Bicerano, J.; Ovshinsky, S. R. Chemical Bond Approach to the Structures of Chalcogenide Glasses with Reversible Switching Properties. *J. Non-Cryst. Solids* **1985**, *74*, 75−84.
(44) Wang, T.; Wang, R. P.; Luther-Davies, B. EXAFS Study of the Local Order in Ge-As-Se Glasses. *Phys. Procedia* **2013**, *48*, 89−95.
(45) Chen, Y.; Xu, T.; Shen, X.; Wang, R. P.; Zong, S.; Dai, S.; Nie, Q. Optical and Structure Properties of Amorphous Ge-Sb-Se Films for Ultrafast All-Optical Signal Processing. *J. Alloys Compd.* **2013**, *580*, 578−583.
(46) Wei, W. H.; Wang, R. P.; Shen, X.; Fang, L.; Luther-Davies, B. Correlation between Structural and Physical Properties in Ge−Sb−Se Glasses. *J. Phys. Chem. C* **2013**, *117*, 16571−16576.
(47) Wei, W. H.; Xiang, S.; Xu, S. W.; Fang, L.; Wang, R. P. Structural Investigation on $Ge_xSb_{10}Se_{90-x}$ Glasses Using X-Ray Photoelectron Spectra. *J. Appl. Phys.* **2014**, *115*, No. 183506.

DOI: 10.1021/acs.jpcb.6b05996
J. Phys. Chem. B 2016, 120, 9204−9214

(48) Gunasekera, K.; Boolchand, P.; Micoulaut, M. Elastic Phases of $Ge_xSb_xSe_{100-2x}$ Ternary Glasses Driven by Topology. *J. Phys. Chem. B* **2013**, *117*, 10027−10034.
(49) Sati, D. C.; Kovalskiy, A.; Golovchak, R.; Jain, H. Structure of $Sb_xGe_{40-x}Se_{60}$ Glasses around 2.67 Average Coordination Number. *J. Non-Cryst. Solids* **2012**, *358*, 163−167.
(50) Lippens, P. E.; Jumas, J. C.; Olivier-Fourcade, J.; Aldon, L. EXAFS Study of the Local Structure in Ge−As−Te Glasses. *J. Non-Cryst. Solids* **2000**, *271*, 119−125.
(51) Drakopoulos, M.; Connolley, T.; Reinhard, C.; Atwood, R.; Magdysyuk, O.; Vo, N.; Hart, M.; Connor, L.; Humphreys, B.; Howell, G.; et al. I12: The Joint Engineering, Environment and Processing (JEEP) Beamline at Diamond Light Source. *J. Synchrotron Radiat.* **2015**, *22*, 828−838.
(52) Hart, M. L.; Drakopoulos, M.; Reinhard, C.; Connolley, T. Complete Elliptical Ring Geometry Provides Energy and Instrument Calibration for Synchrotron-Based Two-Dimensional X-Ray Diffraction. *J. Appl. Crystallogr.* **2013**, *46*, 1249−1260.
(53) Basham, M.; Filik, J.; Wharmby, M. T.; Chang, P. C. Y.; El Kassaby, B.; Gerring, M.; Aishima, J.; Levik, K.; Pulford, B. C. A.; Sikharulidze, I.; et al. Data Analysis WorkbeNch (DAWN). *J. Synchrotron Radiat.* **2015**, *22*, 853−858.
(54) Qiu, X.; Thompson, J. W.; Billinge, S. J. L. PDFgetX2: A GUI-Driven Program to Obtain the Pair Distribution Function from X-Ray Powder Diffraction Data. *J. Appl. Crystallogr.* **2004**, *37*, 678−678.
(55) Kendig, A. P.; Pings, C. J. X-Ray Absorption Factors for Cylindrical Samples in Annular Sample Cells Exposed to Incident Beams of Limited Width. *J. Appl. Phys.* **1965**, *36*, 1692.
(56) Faber, T. E.; Ziman, J. M. A Theory of the Electrical Properties of Liquid Metals. *Philos. Mag.* **1965**, *11*, 153−173.
(57) Warren, B. E. *X-Ray Diffraction*, 2nd ed.; Dover Publications, Inc.: New York, 1990.
(58) Krogh-Moe, J. A Method for Converting Experimental X-Ray Intensities to an Absolute Scale. *Acta Crystallogr.* **1956**, *9*, 951−953.
(59) Norman, N. The Fourier Transform Method for Normalizing Intensities. *Acta Crystallogr.* **1957**, *10*, 370−373.
(60) Egami, T.; Billinge, S. J. L. *Underneath the Bragg Peaks: Structural Analysis of Complex Materials*; Pergamon, Elsevier: Oxford, 2003.
(61) Gereben, O.; Jóvári, P.; Temleitner, L.; Pusztai, L. A New Version of the RMC + + Reverse Monte Carlo Programme, Aimed at Investigating the Structure of Covalent Glasses. *J. Optoelectron. Adv. Mater.* **2007**, *9*, 3021−3027.
(62) Klementev, K. V. Extraction of the Fine Structure from X-Ray Absorption Spectra. *J. Phys. D: Appl. Phys.* **2001**, *34*, 209−217.
(63) McGreevy, R. L.; Pusztai, L. Reverse Monte Carlo Simulation: A New Technique for the Determination of Disordered Structures. *Mol. Simul.* **1988**, *1*, 359−367.
(64) Ankudinov, A. L.; Ravel, B.; Rehr, J. J.; Conradson, S. D. Real-Space Multiple-Scattering Calculation and Interpretation of X-Ray-Absorption near-Edge Structure. *Phys. Rev. B* **1998**, *58*, 7565−7576.
(65) Winterer, M. Reverse Monte Carlo Analysis of Extended X-Ray Absorption Fine Structure Spectra of Monoclinic and Amorphous Zirconia. *J. Appl. Phys.* **2000**, *88*, 5635−5644.
(66) Klementev, K. V. Package "VIPER (Visual Processing in EXAFS Researches) for Windows.". *Nucl. Instrum. Methods Phys. Res., Sect. A* **2000**, *448*, 299−301.
(67) Salmon, P. S. Structure of Liquids and Glasses in the Ge-Se Binary System. *J. Non-Cryst. Solids* **2007**, *353*, 2959−2974.
(68) Pethes, I.; Chahal, R.; Nazabal, V.; Prestipino, C.; Trapananti, A.; Pantalei, C.; Beuneu, B.; Bureau, B.; Jóvári, P. Short Range Order in Ge-Ga-Se Glasses. *J. Alloys Compd.* **2015**, *651*, 578−584.
(69) Itoh, K. Short- and Medium-Range Order in Sb−Se Glasses. *J. Solid State Chem.* **2016**, *233*, 368−373.
(70) Kavetskyy, T.; Shpotyuk, O.; Kaban, I.; Hoyer, W. Radiation-Modified Structure of $Ge_{25}Sb_{15}S_{60}$ and $Ge_{35}Sb_5S_{60}$ Glasses. *J. Chem. Phys.* **2008**, *128*, No. 244514.
(71) The Periodic Table by WebElements https://www.webelements.com/ (accessed Jun 13, 2016).
(72) Cargill, G. S.; Spaepen, F. Description of Chemical Ordering in Amorphous Alloys. *J. Non-Cryst. Solids* **1981**, *43*, 91−97.
(73) Gazzillo, D.; Pastore, G.; Enzo, S. Chemical Short-Range Order in Amorphous Ni-Ti Alloys: An Integral Equation Approach with a Non-Additive Hard-Sphere Model. *J. Phys.: Condens. Matter* **1989**, *1*, 3469−3487.
(74) Cowley, J. M. X-Ray Measurement of Order in Single Crystals of Cu_3Au. *J. Appl. Phys.* **1950**, *21*, 24.

DOI: 10.1021/acs.jpcb.6b05996
J. Phys. Chem. B 2016, 120, 9204−9214